

BEAM SIZE AND INTENSITY DIAGNOSTICS FOR A SRF PHOTOELECTRON INJECTOR

R. Barday*, A. Jankowiak, T. Kamps, A. Matveenko, M. Schenk, F. Siewert, J. Völker,
 Helmholtz-Zentrum Berlin für Materialien und Energie GmbH, Germany
 J. Teichert, Helmholtz-Zentrum Dresden-Rossendorf, Germany

Abstract

A high brightness photoelectron injector must be developed as a part of the BERLinPro ERL program [1, 2]. The injector is designed to produce an electron beam with 100 mA average current and a normalized emittance of 1 mm-mrad. Prior to reaching the final gun/cathode design a staged SRF gun development program has been undertaken which began with the operation of a fully superconducting injector utilizing a lead photocathode. This will be followed by a normal conducting CsK₂Sb cathode capable of generating high current beams. In the first stage we have measured the fundamental beam parameters bunch charge, beam energy and energy spread with a special focus on the measurement of the transverse beam profiles. We will also discuss our plans for the beam characterization at high currents.

INTRODUCTION

In the first stage of the high brightness photoinjector R&D [3, 4] the electron beam is produced from a Pb photocathode in a superconducting RF gun cavity operating at 1.3 GHz. A superconducting lead photocathode was initially directly deposited on the back wall of the gun cavity and irradiated by a UV laser operated at 258 nm with 2-3 ps pulse duration. The maximum average beam current extracted from this gun was 50 nA corresponding to a bunch charge of about 6 pC. The maximum beam energy of about 2.0 MeV was achieved at a peak field on the cathode of 22 MV/m.

In the second version of this type of the SRF gun, a thin layer of lead with a diameter of 5 mm and a thickness of about 400 nm was deposited on a Nb plug, which can be inserted into the backplane of the cavity. The plug is vacuum sealed with an indium gasket. The advantage of this design is a possibility to change the photocathodes and to test different deposition methods. The gun cavity with the coated plug was tested up to the peak fields on the cathode of 35 MV/m without laser irradiation [5].

DIAGNOSTICS BEAMLINE

A schematic overview of the diagnostics beamline is shown in Fig. 1. A dipole spectrometer magnet is used to measure the beam energy and the energy spread. To improve the energy resolution we installed a vertical slit made

of copper in the dispersive arm with a width of 2 mm and a thickness of 4 mm.

Measuring the low energy electrons utilizing a Faraday cup can be challenging due to backscattering of primary electrons and secondary electron emission. The number of backscattered electrons per incident electron for primary electrons with energy of 1 MeV impinging on a copper target is about 0.23 [6]. The secondary and backscattered electrons can be trapped if the Faraday cup has a sufficient large ratio of length to diameter, which is commonly not practical. Alternatively the Faraday cup can be electrically biased to suppress low energy electrons, which is the case in our beamline. The bunch charge is measured with an integrating current transformer (ICT).

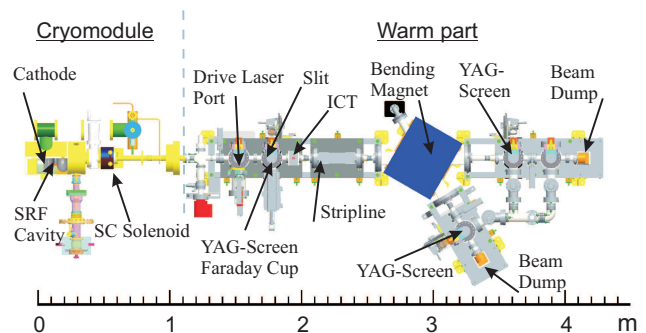


Figure 1: Schematic view of the diagnostics beamline.

An electron beam is visualized by the image of the scintillation light emitted by the cerium-doped yttrium aluminium garnet (YAG:Ce) crystal with Ce-doping concentration of 0.2 %. YAG is a vacuum friendly material with a short decay time and high light output of ~35 photons per keV of absorbed energy. In order to avoid accumulation of the absorbed electric charge in the crystal, a thin, 10 nm, Indium Tin Oxide (ITO) coating was applied. ITO has high electrical conductivity and is optically transparent. Initial tests with an uncoated YAG crystal irradiated by low energy electrons showed damage, which look like fine scratches shown in Fig. 2.

To provide a better control of the electron beam and to avoid collisions between the Faraday cup and the view screen (which happened in the first version of the beamline with a YAG screen installed perpendicular to the Faraday cup), the YAG:Ce was incorporated into the Faraday cup (Fig. 3). In this design the free standing view screen with a diameter of 32 mm and a thickness of 100 μm was mounted at a 45 degree angle with respect to the incoming

* roman.barday@helmholtz-berlin.de

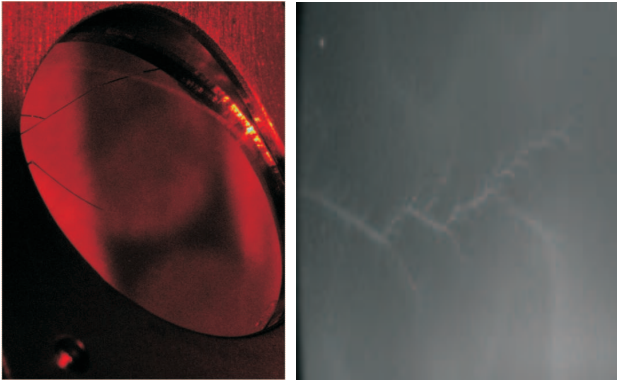


Figure 2: Photograph of the view screen after collision with the Faraday cup on the left and scratches on the uncoated view screen from low energy electrons on the right.

beam. A 45 degree mirror located in the accelerator plane perpendicular to the beam direction reflects the beam image onto a charge-coupled device (CCD) camera [7]. The camera is mounted vertically below the accelerator plane to minimize its damage due to radiation. The CCD-Camera is sensitive to the light within the range of 400 to 1000 nm which has a maximum at 500 nm and is well suited for the detection of the scintillation light from the YAG:Ce with a maximum radiation wavelength of 550 nm. The CCD chip has dimensions of 659X494 pixels with a pixel size of 9.9X9.9 μm and is digitized with a 12 bit ADC.

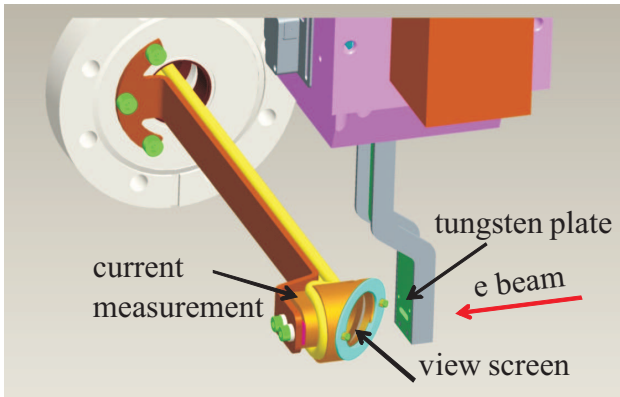


Figure 3: Schematic view of the Faraday cup with a YAG:Ce view screen and a slit.

Transverse Beam Profile

The beam emittance can be measured using a standard solenoid scanning technique, where the transverse beam size is measured for different focal lengths of the solenoid. An example of the solenoid scan is shown in Fig. 4. The electron beam was focused to waists of $\sim 350 \mu\text{m}$ [8].

Additionally, the transverse emittance can be measured using a single slit mask and a view screen while keeping the focal length of the solenoid fixed. A horizontal slit in a tungsten plate with a width d of 0.1 mm and a thickness of 1.5 mm provides a compromise between requirements

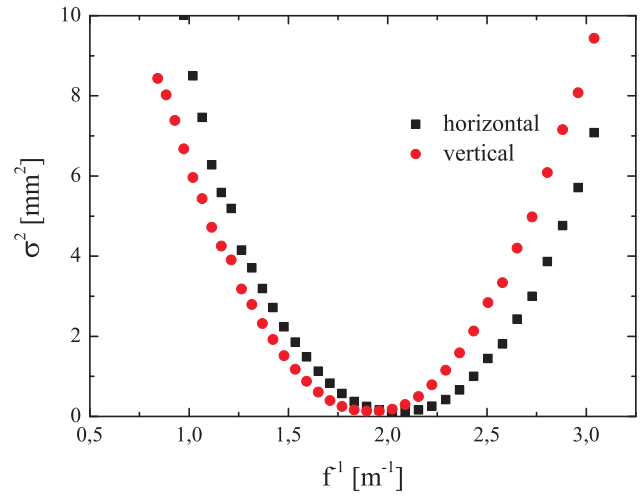


Figure 4: Example of the solenoid scan.

on a good resolution and a tolerance of the angular alignment. The stopping power of tungsten at the beam energy of 1 MeV is 19.3 MeVcm²/g, so that we expect a sufficient suppression of the background.

Both techniques are based on the precise beam size measurement, so, the spatial resolution of the view screens is a critical point. The scintillation mechanism involving following phases [9]:

- energy conversion
- thermalization of electrons and holes
- energy transfer to the luminescent centers
- photon emission at the scintillating sites

can limit the scintillator resolution. Here we consider only the geometric effects and an interaction of the primary beam with the view screen and not the processes of the light generation. For a low energy electron beam the spatial resolution of the screen can be limited by multiple Coulomb scattering of electrons in the screen. If we ignore single electron scattering at large angle, the multiple scattering angle of electrons penetrating through a material with a radiation length of Z_0 is given by [10]

$$\theta_{\text{rms}} = \frac{13.6\text{MeV}}{\beta pc} \sqrt{\frac{z}{Z_0}} \left(1 + 0.038 \ln \frac{z}{Z_0} \right), \quad (1)$$

where p is the electron momentum, βc is the velocity of the particles and z/Z_0 is the thickness of the material in radiation lengths ($Z_0=3.5$ cm for YAG:Ce). For a point electron source with beam energy of 1 MeV the RMS size of the electron beam at the exit of the screen with an effective thickness of $z=\sqrt{2}d$ can be estimated as

$$\sqrt{2 \int \int \theta_{\text{rms}}^2 dz' dz} \sim \frac{13.6\text{MeV}}{\beta pc} \sqrt{\frac{z^3}{3Z_0}} \sim 53\mu\text{m}. \quad (2)$$

However, the electron beam appears for the CCD-Camera with an RMS size of

$$y_{\text{rms}} \sim \frac{13.6\text{MeV}}{\beta pc} \sqrt{\frac{z^3}{12Z_0}}, \quad (3)$$

giving a spatial resolution of the screen in the vertical plane of $26\ \mu\text{m}$. Here we neglected the electron energy loss and assumed a homogeneous emission of the scintillated light along the scintillator.

In the horizontal plane an effective beam size seen by the camera due to the tilt of the screen (Fig. 5) can be estimated for our geometry as

$$X_{\text{eff}} = \frac{d + \delta}{\sqrt{2}} = \frac{d}{\sqrt{2}} \left(1 + \frac{1}{\sqrt{2n^2 - 1}} \right), \quad (4)$$

where n is the index of refraction. Equation 4 shows that the screen thickness has a significant influence on the spatial resolution in the horizontal plane. From this point of view, materials with a large index of reflection, like BGO with $n=2.15$, or diamond with $n=2.4$, provide a better spatial resolution, but the influence of the reflection index is weak. For the YAG:Ce view screen with an index of reflection $n=1.82$ the beam size seen by the camera for a point electron beam is limited by the thickness of the scintillator $X_{\text{eff}} \sim d$. This corresponds to the minimum RMS size in the horizontal plane $x_{\text{rms}} = X_{\text{eff}}/\sqrt{12} \sim 30\ \mu\text{m}$. Additionally, multiple Coulomb scattering also contributes to the beam size, so that the screen resolution in the horizontal plane for an electron beam with a finite beam size is larger than $30\ \mu\text{m}$ estimated for a point electron beam without scattering.

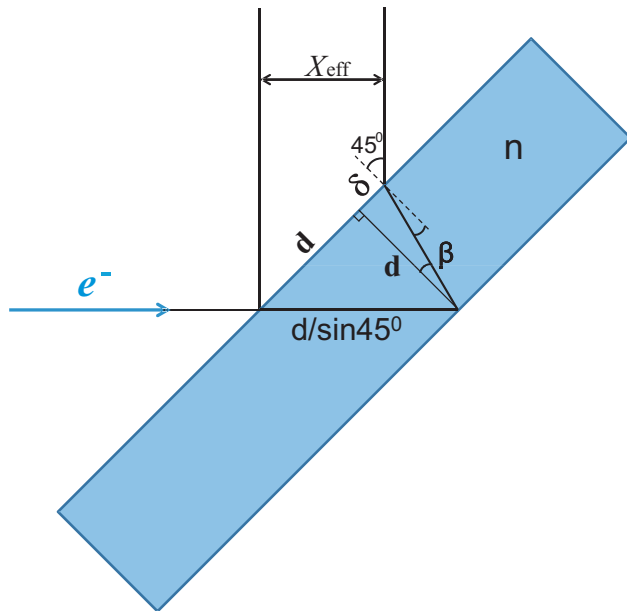


Figure 5: Beam size seen by the camera in the horizontal plane for a point electron beam.

BEAM CHARACTERIZATION AT HIGH BEAM INTENSITY

A test of the view screens at high beam intensity was performed at Helmholtz-Zentrum Dresden Rossendorf. An electron beam with a momentum of $15\ \text{MeV}/c$ passes

through a thin beryllium vacuum window and hits a view screen (Fig. 6). Two different materials were investigated as a view screen: a free standing chemical vapor deposited (CVD) diamond with a thickness of $150\ \mu\text{m}$ and a free standing YAG:Ce crystal with a thickness of $200\ \mu\text{m}$. A mirror reflects the scintillation light into a CCD-Camera oriented at ~ 155 degree angle with respect to the incoming beam. A CVD-diamond has an excellent thermal conductivity of $\sim 2000\ \text{W}/(\text{mK})$, which is two orders of magnitude higher than for YAG:Ce and is well suited for the visualization of the beam with high intensity.

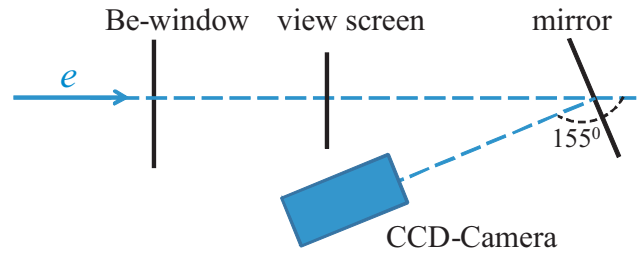


Figure 6: Layout of the experimental setup.

In this experiment the electron gun operated with $0.1\ \text{ms}$ and $1.0\ \text{ms}$ long macropulses separated by $1\ \text{s}$. Within the macropulse the bunch repetition rate was changed between 0.1 and $26\ \text{MHz}$ at a bunch charge of $\sim 20\ \text{pC}$ giving a macropulse charge between 0.2 and $290\ \text{nC}$. The light intensity for both screens was measured as a function of the macropulse charge. Both screens showed a linear dependence from the charge, but YAG provides light output two orders of magnitude higher than diamond for the same settings of the CCD-Camera as shown in Fig. 7. An example of the beam profile measurement is shown in Fig. 8. No optical attenuator was used between the screen and the CCD-Camera in this measurement.

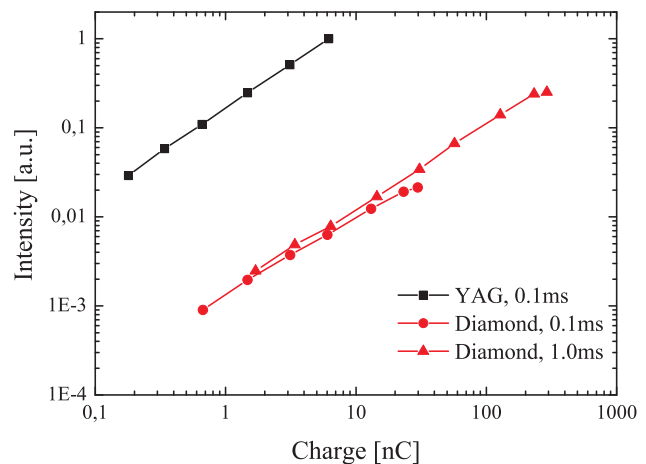


Figure 7: Light output intensity measured with a CVD-diamond and a YAG:Ce scintillator.

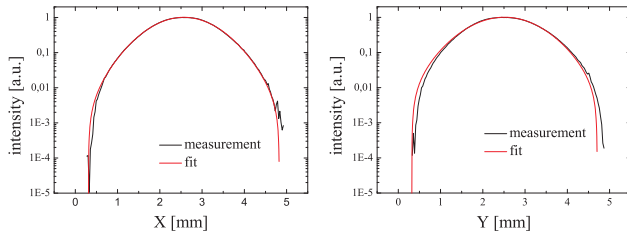


Figure 8: Beam profile measurement using a YAG:Ce view screen and a Gaussian fit.

Optical Measurements

A white-light interferometer (magnification 20X) was employed to measure the surface roughness of the CVD-diamond. Figure 9a shows an unpolished side of the diamond, which is formed from the polished silicon wafer on which it is grown. The ridges with a transverse size of about $10\ \mu\text{m}$ and a height of several nanometer are due to the polishing of the silicon wafer. Figure 9b shows a polished side of the diamond, which is free of such artifacts, but the peak-to-peak roughness is about a factor of 4 worse. Such structures can scatter the light and have a potential to affect the spatial resolution at a beam size comparable to the size of the ridges. After the irradiation of the diamond screen with an electron beam no surface damage was observed.

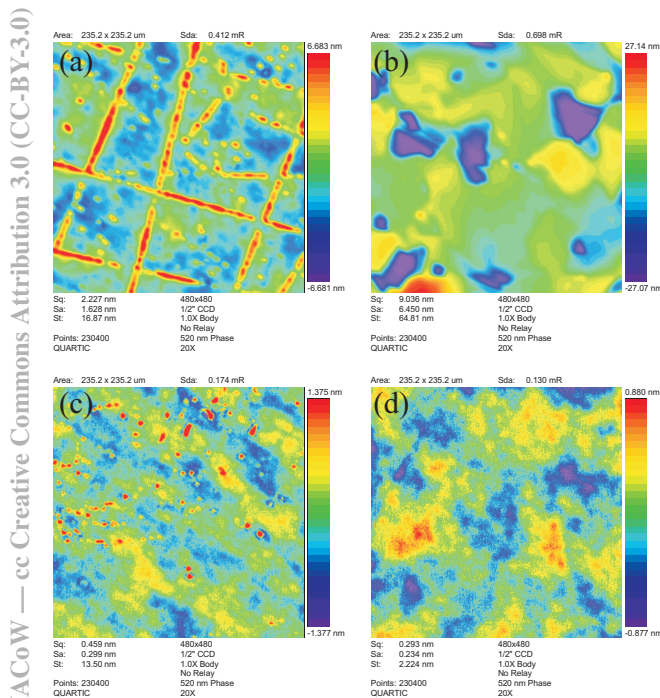


Figure 9: Unpolished (a) and polished (b) sides of the CVD-diamond; front (c) and back (d) sides of the YAG:Ce crystal.

FUTURE DEVELOPMENTS AT HZB

An implementation of the CsK_2Sb cathode will allow a production of the electron beam with an average current of up to 100 mA and bunch charge of 77 pC at 1.3 GHz repetition rate. YAG:Ce crystal provides a high light output and is suitable for the beam visualization at low intensity, but it has a moderate spatial resolution [11]. YAG:Ce exhibits a decay time of $\sim 70\ \text{ns}$, which is longer than the distance between the bunches at 1.3 GHz. At a charge density of $\sim 0.01\ \text{pC}/\mu\text{m}^2$ a saturation blurring appears due to limited amount of Ce sites available for emission. We want to study the influence of the Ce activator concentration varying from 0.1 to 0.2% in the YAG crystal on the spatial resolution and saturation effect which occurs at high charge density. We want to install a screen holder with five different view screens (Fig. 10) to compare a spatial resolution of a standard YAG:Ce, LuAG:Ce, CRY19 (trade name from CRYTUR), CVD-diamond with a wire scanner serving as a reference signal. The wire scanner utilizes a tungsten wire with a diameter of $40\ \mu\text{m}$. At high beam intensity a CVD-diamond screen is preferable and we want to study the influence of the radiation damage on the efficiency of the radiator at high intensity.

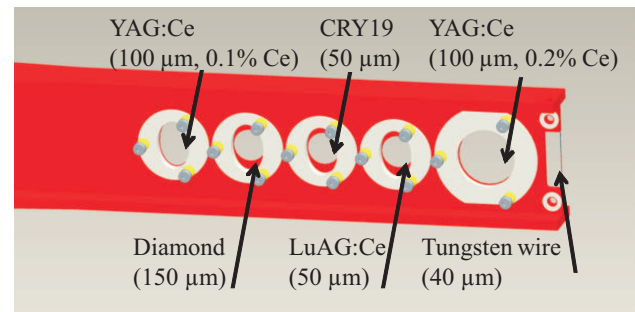


Figure 10: Holder for the view screens investigation.

The transverse beam size at high currents will be also measured using a double slit system with a shield to protect the precise slit at high beam power based on the Cornell design [12].

ACKNOWLEDGMENTS

The authors acknowledge fruitful discussions with A. Bondarenko, A. Burrill, G. Kube and D. Böhlick. Work supported by Bundesministerium für Bildung und Forschung and Land Berlin.

REFERENCES

- [1] A. Jankowiak *et al.*, Proceedings of LINAC'10, TUP007, p. 407.
- [2] J. Knobloch *et al.*, Proceedings of IPAC'12, MOPPP015, p. 601.
- [3] T. Kamps *et al.*, Proceedings of IPAC'11, THPC109, p. 3143.

- [4] A. Neumann *et al.*, Proceedings of IPAC'11, MOODA03, p. 41.
- [5] J. Sekutowicz, Proceedings of EuCARD'12.
- [6] R. Ito *et al.*, Rad. Phys. Chem. 42 (1993) 761.
- [7] <http://www.baslerweb.com>
- [8] J. Völker *et al.*, Proceedings of IPAC'12, TUPPD051, p. 1518.
- [9] P. Lecoq *et al.*, *Inorganic Scintillators for Detector Systems*, (Springer Verlag, Berlin-Heidelberg, 2006).
- [10] G.R. Lynch *et al.*, NIM B58 (1991) 6.
- [11] G. Kube *et al.*, Proceedings of IPAC'12, WEOAA02, p. 2119.
- [12] I.V. Bazarov *et al.*, Phys. Rev. ST Accel. Beams 11 (2008) 100703.